EARTH SURFACE PROCESSES AND LANDFORMS, VOL 23, 171–191 (1998)

TIME-AVERAGED FLOW STRUCTURE IN THE CENTRAL REGION OF A STREAM CONFLUENCE

BRUCE L. RHOADS[1*] AND STEPHEN T. KENWORTHY[2]

[1]*Department of Geography, University of Illinois, Urbana, IL 61801, USA*
[2]*Department of Geography and Environmental Engineering, The Johns Hopkins University, Baltimore, MD 21218-2686, USA*

Received 9 September 1996; Revised 23 January 1997; Accepted 18 March 1997

ABSTRACT

Previous process-oriented field studies of stream confluences have focused mainly on fluvial dynamics at or immediately downstream of the location where the confluent flows enter the downstream channel. This study examines in detail the spatial evolution of the time-averaged downstream velocity, cross-stream velocity, and temperature fields between the junction apex, where the flows initially meet, and the entrance to the downstream channel. A well-defined, vertically oriented mixing interface exists within this portion of the confluence, suggesting that lateral mixing of the incoming flows is limited. The downstream velocity field near the junction apex is characterized by two high-velocity cores separated by an intervening region of low-velocity or recirculating fluid. In the downstream direction, the high-velocity cores move inwards towards the mixing interface and high-velocity fluid progressively extends downwards into a zone of scour, resulting in an increase in flow velocity in the centre of the confluence. The cross-stream velocity field is dominated by flow convergence, but also includes a component associated with a consistent pattern of secondary circulation. This pattern is characterized by two surface-convergent helical cells, one on each side of the mixing interface. The helical cells appear to be the mechanism by which high-momentum fluid near the surface is advected downwards into the zone of scour. For transport-ineffective flows, the dimensions and intensities of the cells are controlled by the momentum ratio of the confluent streams and by the extant bed morphology within the confluence. Although the flow structure of formative events was not measured directly in this study, documented patterns of erosion and deposition within the central region of the confluence suggest that these events are dynamically similar to the measured flows, except for the fact that formative flows are not constrained by, but can reshape, the bed morphology. The results of this investigation are consistent with and augment previous findings on time-averaged flow structure in the downstream portion of the confluence. © 1998 John Wiley & Sons, Ltd.

Earth surf. process. landforms, **23,** 171–191 (1998)
No. of figures: 12 No. of tables: 1 No. of refs: 33
KEY WORDS: stream confluences; flow structure; helical flow

INTRODUCTION

As water moves through a drainage network, it is forced to converge at stream confluences. This forced convergence of flow produces a complex hydrodynamic environment, or confluence hydrodynamic zone (CHZ) (Kenworthy and Rhoads, 1995), within the immediate vicinity of the junction. Until recently, relatively little was known about the dynamics of flow through confluences or the relationship of local hydrodynamic conditions to confluence geomorphology. Over the past several years a considerable body of theoretical (Weerakoon *et al*., 1991), experimental (Best, 1987, 1988; Best and Roy, 1991; McLelland *et al*., 1996; Biron *et al*., 1996a,b) and field (Roy and Bergeron, 1990; Ashmore *et al*., 1992; Biron *et al*., 1993b; Bristow *et al*., 1993; Rhoads and Kenworthy, 1995; Gaudet and Roy, 1995; Rhoads, 1996) research has emerged on the fluvial dynamics of stream confluences. This work has begun to reveal the complex three-dimensionality of the turbulent and time-averaged flow fields at confluences. It has also suggested that coherent flow structures of various scales can exist at confluences and that the presence or absence of particular structures can vary both from confluence to confluence and from time to time at a specific confluence (e.g. Biron *et al*., 1993a; Rhoads

Correspondence to: B. L. Rhoads
Contract grant sponsor: National Science Foundation; contract grant number: SES-9024225
Contract grant sponsor: University of Illinois Research Board.

CCC 0197-9337/98/020171–21 $17.50 © 1998 John Wiley & Sons, Ltd.

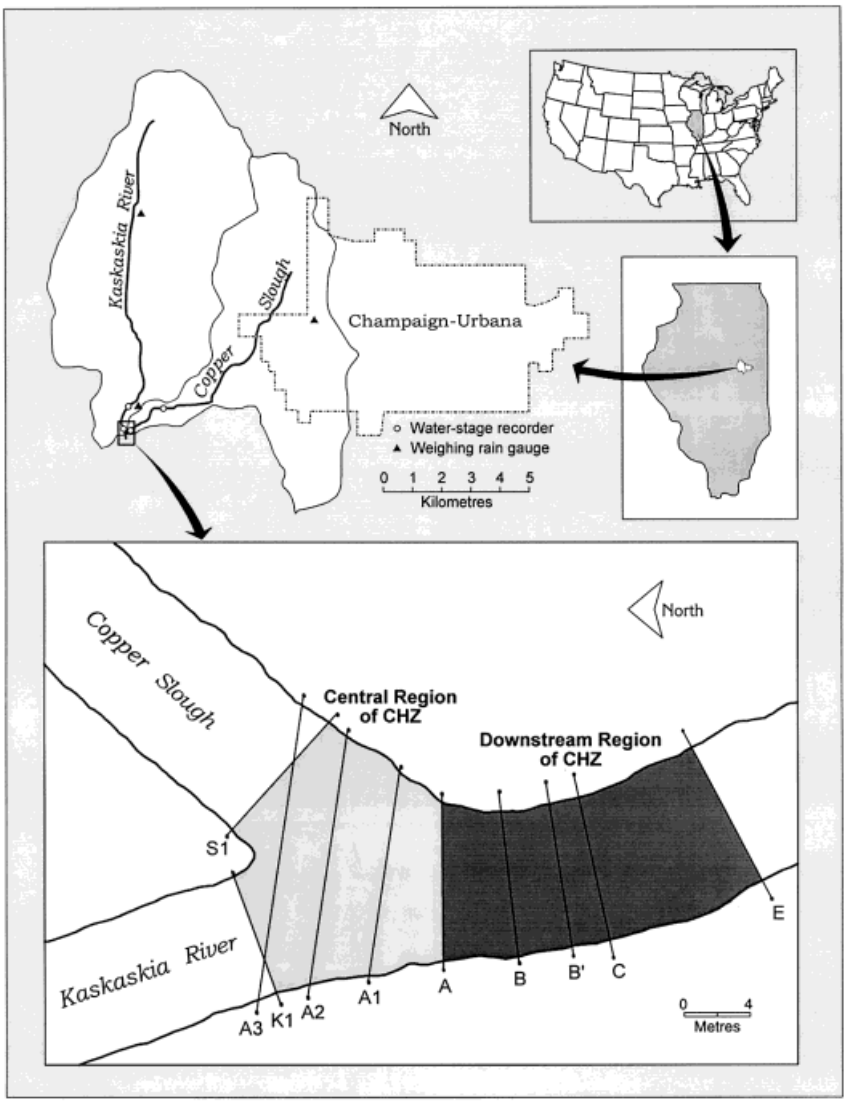

Figure 1. Map of study site showing central and downstream regions of the confluence hydrodynamic zone (CHZ) and the locations of measurement cross-sections

and Kenworthy, 1995; McLelland *et al*., 1996). Despite these advances, knowledge of time-averaged and turbulent flow at confluences is incomplete. Additional field and laboratory measurements are needed to characterize the full variety of hydrodynamic features that can occur at confluences, to link these features to controlling factors such as planform geometry and hydrologic conditions, and to establish the relative influence of various hydrodynamic features on spatial patterns of shear stress, bedload transport, bed-material characteristics, and bed morphology.

This paper examines the time-averaged, two-dimensional (downstream and cross-stream) flow structure within the central region of the CHZ at a small stream confluence with an asymmetrical planform (i.e. the receiving channel is a linear extension of one of the upstream tributaries). The study complements previous research focusing on the time-averaged flow structure in the downstream portion of the CHZ at this confluence (Rhoads and Kenworthy, 1995; Rhoads, 1996). Specifically, this investigation explores the spatial evolution of the time-averaged flow field between the junction apex and the location where flow from the confluent streams

 © 1998 John Wiley & Sons, Ltd.

enters the downstream channel. It also examines how flow structure in this part of the CHZ varies with changes in hydrologic conditions and bed morphology. A particular focus of this research is to document the presence or absence of time-averaged, helical motion in the central region of the confluence. The existence of helical motion at confluences, the mechanism by which this motion, if present, is generated, and the role of helical motion in confluence dynamics are issues that have yet to be fully resolved (Rhoads and Kenworthy, 1995; Rhoads, 1996; McLelland *et al*., 1996; Biron *et al*., 1996a,b).

FIELD SITE

The study site is the confluence of the Kaskaskia River and Copper Slough located in the headwaters of the Kaskaskia River basin in east-central Illinois, USA (Figure 1). The confluence is asymmetrical in planform with a junction angle of approximately 60°. The Kaskaskia River drains 54 km^2 of rural farmland upstream of the confluence, whereas the Copper Slough has a basin area of 41 km^2 and receives runoff from the western portion of Champaign, as well as from agricultural fields. Both streams have been channelized and are contained within large trapezoidal ditches with steep (>30°), heavily vegetated, soil-mantled banks. Top widths of the ditches range from 15 to 17 m and depths are between 3 and 4 m. Inset channels carved by low flows exist at the bottom of the ditches. These inset channels, which are clearly demarcated by an abrupt change in the gradient of each ditch bank and by the absence of vegetation on the lower part of the banks, are 7 to 9 m wide and 0·25 to 0·3 m deep. Average channel gradients upstream of the confluence are 0·0005 for the Kaskaskia River and 0·0011 for the Copper Slough. Bed material in the Copper Slough consists of bimodal sand and gravel with a median grain size (D_{50}) of 2 to 3 mm, whereas the bed of the Kaskaskia River upstream of the confluence comprises unimodal sand (D_{50} = 0·5 to 0·7 mm). The composition of bed material in the downstream channel varies with the relative input of sediment from each of the upstream channels (Mayer, 1995; Rhoads, 1996).

FIELD DATA

Previous research at the Kaskaskia River–Copper Slough confluence has focused on flow structure at and immediately downstream of the location where flow enters the post-confluence channel (Figure 1). During the summer of 1993, measurements of the time-averaged flow field were obtained on three dates, 7 June, 8 July and 27 July, in the region where the confluent streams initially meet. The upstream and downstream limits of this region are defined by the junction apex and the downstream junction corner, respectively (Figure 1).

Hydraulic conditions in the upstream channels were determined at two cross-sections (S1 and K1) approximately 1 m upstream of the junction (Figure 1). Flow velocities and water temperatures were measured at 0·5 m intervals across the channel at a height of 0·6D below the water surface, where D is the local flow depth. These data were used to compute the discharges (Q, m^3 s^{-1}), cross-sectional average velocities ($\overline{V}$, m s^{-1}), average temperatures (T, °C), and momentum flux ratio (M_r) of the incoming flows:

$$M_r = (\rho Q_c \overline{V}_c)/(\rho Q_k \overline{V}_k)$$

where ρ is water density (1000 kg m^{-3}), and the subscripts c and k denote the Copper Slough and Kaskaskia River, respectively. In addition to these measurements, flow stages and water temperatures of the two streams were monitored at 60 min intervals throughout each day at two gauging stations located 15 m upstream of the confluence.

Detailed measurements of flow velocities and water temperatures were obtained at four cross-sections spanning the central portion of the confluence (Figure 1). These cross-sections are spaced 3 to 4 m apart and are orthogonal either to the junction-angle bisector (cross-sections A1–A3) or to the local channel centreline (cross-section A). The downstream cross-section in this study (cross-section A) corresponds to the upstream cross-section in previous research focusing on flow structure in the downstream portion of the CHZ (Rhoads and Kenworthy, 1995; Rhoads, 1996).

Measurements of downstream velocities (v_x) and cross-stream velocities (v_y) were obtained at several verticals along each of the four cross-sections within the confluence using a Marsh–McBirney Model 511 electromagnetic current meter (time constant 0·2 s). Measurements at cross-section A3 were bounded by cross-

© 1998 John Wiley & Sons, Ltd.

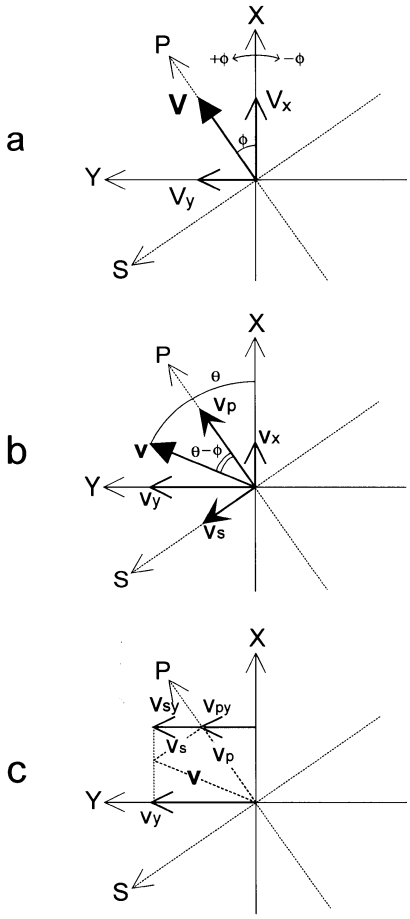

Figure 2. Diagram illustrating (a) relations among depth-averaged downstream velocity (V_x), depth-averaged cross-stream velocity (V_y), and depth-averaged resultant velocity ($\boldsymbol{V}$) at a vertical; (b) relations among the mean downstream velocity (v_x), mean cross-stream velocity (v_y), mean resultant velocity ($\boldsymbol{v}$), the primary velocity (v_p) and the secondary velocity (v_s) at a point in a vertical; and (c) relations among v_s, v_p, $\boldsymbol{v}$, v_y, the cross-stream component of the primary velocity (v_{py}) and the cross-stream component of the secondary velocity (v_{sy}). Coordinate systems X, Y and P, S correspond to the downstream/cross-stream and primary/secondary flow directions, respectively

sections K1 and S1, whereas those at the other cross-sections extended across the width of flow. The electromagnetic sensor and a YSI thermistor probe (precision ±0·02°C) were mounted on a custom-built wading rod, which in turn was attached to a steel cable strung between the end points of the cross-section and then plumbed using a rod level. This mounting system ensured that the X-axis of the sensor head was oriented orthogonally to each cross-section at each vertical. Because ratchets were used to tighten the steel cable, the wading rod was highly stable and did not vibrate or oscillate during the period of measurement.

The number of measurement locations per cross-section ranged from 30 to 50 with an average of 40. The number of locations at a vertical varied directly with flow depth, ranging from two (D<0·10 m) to eight (D>0·60 m). In general, the spacing of measurement locations was adjusted so that the sensing volume of the flow sensor (5·7 cm from the centre of the probe) sampled most of the fluid between the bed and the surface at each vertical. At each point in a vertical profile, the outputs of the current meter and temperature probe were sampled at 5 Hz over an interval of 60 s. Previous work at this confluence has shown that a 60 s interval is adequate for characterizing the time-averaged velocity within the mixing interface, which contains coherent eddies that produce systematic velocity fluctuations with a periodicity of 10 to 15 s (Kenworthy, 1994). Uncertainty (σ) in time-averaged velocities associated with long-term zero drift, linearity of response, wideband electronic noise, and absolute calibration of the current meter can be estimated by:

 © 1998 John Wiley & Sons, Ltd.

$$\sigma = \xi/\sqrt{N}$$

where ξ is the uncertainty of an individual measurement and N is the number of measurements (Bevington, 1969, p. 71). The accuracy of the current meter for an individual measurement is about $\pm 0{\cdot}04\,\mathrm{m\,s^{-1}}$; thus the estimated uncertainty in mean velocities is less than $\pm 0{\cdot}003\,\mathrm{m\,s^{-1}}$

Each cross-section (including K1 and S1) was surveyed immediately prior to obtaining the flow measurements, taking care not to disturb the bed. Because the morphology of the channel bed did not change during the period of flow measurement, these survey data can be used to determine the spatial pattern of bed topography within the confluence on each date.

ANALYSIS OF VELOCITY DATA

The study of flow structure in natural rivers requires a coordinate system, or frame of reference, for analysis and presentation of velocity fields. The choice of a particular frame of reference depends upon the objectives of an investigation and the nature of the flow field of interest. An objective of this study is to characterize how two types of fluid motion – skewing of the flow and helical motion, if present – contribute to the cross-stream velocity field at a confluence, where the orientation of each cross-section remains fixed. Because flow at confluences is strongly convergent, most time-averaged velocity vectors will be oriented at oblique angles to the orientations of fixed cross-sections. In addition, helical motion may exist within the flow producing differences in the degree of obliqueness among individual vectors both at a vertical and throughout the cross-section. The cross-stream velocity field will consist of a combination of these separate types of fluid motion. As flow conditions at a confluence change, the intensities of convergence and helical motion may change, resulting in changes in the cross-stream velocity field. To determine the degree to which these separate types of fluid motion contribute to documented changes in the cross-stream flow field, the velocity component associated with skewing of the flow vectors in relation to the cross-section must be isolated from the component associated with helical motion.

One way to isolate skewed flow from helical motion is to compute velocity components parallel and perpendicular to the depth-averaged velocity vector ($\boldsymbol{V}$) at each vertical; these components are primary velocities (v_p) and secondary velocities (v_s), respectively (Bathurst *et al.*, 1977). The magnitude (V) and orientation (ϕ) of $\boldsymbol{V}$ (Figure 2) are calculated as:

$$V = \sqrt{V_x^2 + V_y^2} \tag{1}$$

$$\phi = \tan^{-1}\left\{\frac{V_y}{V_x}\right\} \tag{2}$$

where V_x is the depth-averaged downstream velocity, V_y is the depth-averaged cross-stream velocity, and values of V_x and V_y are obtained by integrating v_x and v_y over the flow depth (D):

$$V_x = \frac{1}{D}\int_0^D v_x \,\mathrm{d}z \tag{3}$$

$$V_y = \frac{1}{D}\int_0^D v_y \,\mathrm{d}z \tag{4}$$

Values of v_p and v_s are computed as:

© 1998 John Wiley & Sons, Ltd.

$$v_p = v\cos(\theta - \phi) \tag{5}$$

$$v_s = v\sin(\theta - \phi) \tag{6}$$

where v and θ are the magnitude and orientation, respectively, of the resultant velocity vector ($\boldsymbol{v}$) at each measurement position in a vertical (Figure 2):

$$v = \sqrt{v_x^2 + v_y^2} \tag{7}$$

$$\theta = \tan^{-1}\left\{\frac{v_y}{v_x}\right\} \tag{8}$$

When spiral flow is present, values of v_s will systematically decrease or increase over the flow depth and the same vertical pattern of v_s will occur at adjacent verticals (Bathurst *et al*., 1977, 1979). Such patterns of two-dimensional velocities routinely provide the basis for inferring the existence of helical flow in fluvial environments (e.g. Bathurst *et al*., 1979; Thorne and Hey, 1979), including stream confluences (Ashmore *et al*., 1992). A similar strategy was adopted in this study; however, it should be noted that three-dimensional measurements are required to unequivocally establish the presence of helical flow.

In skewed flows, values of $\phi \neq 0$. In certain types of skewed flows, such as those that are convergent or divergent, values of ϕ, and thus the orientations of planes normal to the depth-averaged velocity vectors (S in Figure 2), vary appreciably across the channel. In either case, two-dimensional plots of v_s do not represent flow in the plane of the cross-section (Y in Figure 2), but instead show a composite picture of velocity components parallel to the local plane of reference at each vertical. Only at verticals where $\phi = 0$ will the local plane of orientation and the cross-sectional plane of orientation be equivalent. Moreover, from one hydrologic event to the next, the values of ϕ at each vertical can change. Thus, plots of v_p and v_s cannot be used to evaluate differences in flow structure among events within a fixed frame of reference, or planar 'slice' through the flow. These difficulties can be overcome by calculating the cross-stream components of v_p and v_s (Figure 2):

$$v_{py} = v_p \sin\phi \tag{9}$$

$$v_{sy} = v_s \cos\phi \tag{10}$$

where values of v_{sy} represent the contribution of secondary circulation to the cross-stream velocity field and values of v_{py} represent the component of the cross-stream velocity associated with flow in the direction of the depth-averaged vector at that vertical. The sum of these components is equal to the measured cross-stream velocity (Figure 2).

RESULTS

Hydrologic, hydraulic and morphologic conditions

The record of flow stage at the confluence provides a hydrologic context for the three sets of flow measurements (Figure 3). The stage at baseflow is approximately 0·2 m above the elevation of the pressure transducer (95·93 m, arbitrary datum). The pattern of stage variation above baseflow during June and July 1993

 © 1998 John Wiley & Sons, Ltd.

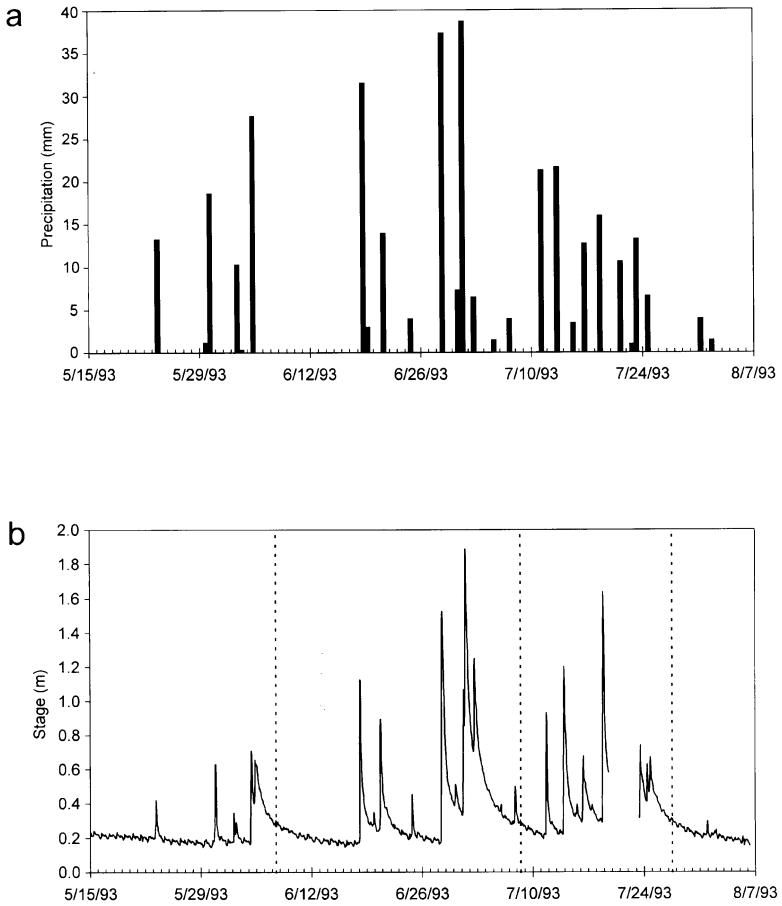

Figure 3. Diagrams showing (a) mean daily precipitation in the upper Kaskaskia River basin and (b) flow stage above the elevation of the pressure transducer (95·93 m, arbitary datum) at the Copper Slough–Kaskaskia River confluence, mid-May to early August 1993 (Dates of measurements are shown as dashed lines)

Table I. Hydraulic conditions at cross-sections K1 and S1

	7 June 1993				8 July 1993				27 July 1993			
	K1	S1	K1+S1	S1/K1	K1	S1	K1+S1	S1/K1	K1	S1	K1+S1	S1/K1
Q	0·88	0·62	1·50	0·70	0·69	0·77	1·46	1·11	0·54	0·92	1·46	1·70
M	338	217	555	0·64	220	314	534	1·43	148	471	619	3·18
$\bar{V}$	0·39	0·35	–	0·90	0·32	0·41	–	1·28	0·27	0·51	–	1·89

Q = discharge ($m^3 s^{-1}$), M = momentum flux ($kg\,m\,s^{-2}$), $\bar{V}$ = mean cross-sectional velocity ($m\,s^{-1}$)

clearly reflects the sequence and magnitude of individual precipitation events. All three sets of flow measurements were obtained during the receding stages of individual hydrologic events.

The three data sets include one flow with $M_r > 1{\cdot}0$, one with $M_r < 1{\cdot}0$, and one with $M_r \approx 1{\cdot}0$ (Table I). In contrast, the total discharges for the three dates were similar ($1{\cdot}45$–$1{\cdot}50\,m^3\,s^{-1}$). Thus, the data provide a framework for assessing the effects of variation in momentum ratio and bed morphology on time-averaged flow structure for a specific total discharge. Although minor backwater effects may have occurred at cross-sections K1 and S1, the similarity between the discharge ratios and momentum ratios for the three dates suggests that these effects were minor and did not seriously distort measurements of the momentum relations between the confluent flows.

© 1998 John Wiley & Sons, Ltd.

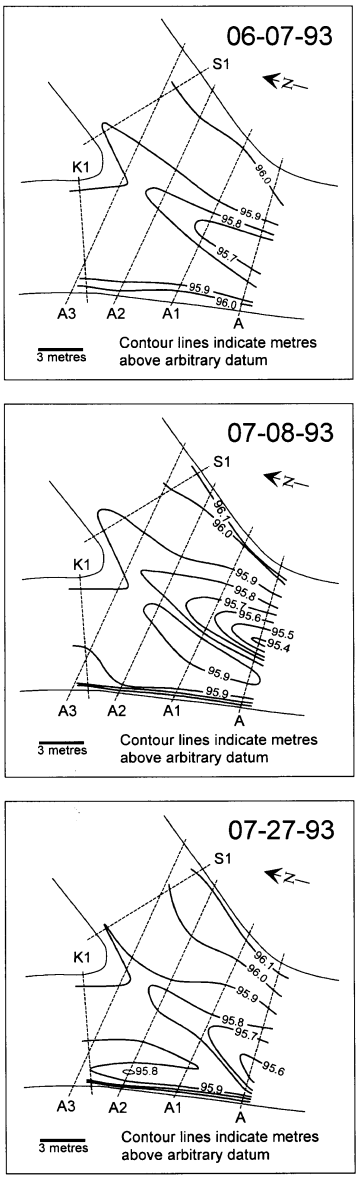

Figure 4. Bed topography at the confluence on the three flow-measurement dates

General morphological features present on all three dates include: (1) an elongated scour hole extending from within the confluence into the downstream channel; (2) a lobe of sand on the west side of the scour hole protruding into the confluence from the Kaskaskia River; and (3) a wedge of gravelly sediment along the east side of the scour hole extending into the confluence from the Copper Slough. The latter two features are similar to the confluence mouth bars described by Bristow *et al*. (1993). On 7 June the scour hole was 0·25 to 0·35 m deep and had side slopes with a maximum gradient (ϕ_m) of 10° (Figure 4). Cross-sectional profiles for this date are fairly symmetrical, with the zone of maximum scour located near the centre of the confluence (Figure 5). Several events with stages 0·8 to 1·6 m above baseflow stage altered the bed morphology between 7 June and 8 July (Figure 3). These events deepened the scour hole by 0·25 m and increased the steepness of its side slopes ($\phi_m = 21°$) (Figure 4). In addition, the axis of the scour hole shifted towards the east bank by approximately 1 m as sand from the Kaskaskia River penetrated further into the confluence (Figure 5). As this wedge of sand

 © 1998 John Wiley & Sons, Ltd.

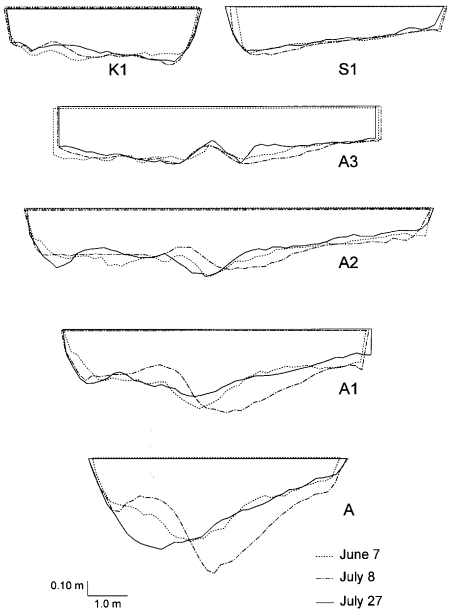

Figure 5. Changes in channel cross-sections between the three flow-measurement dates

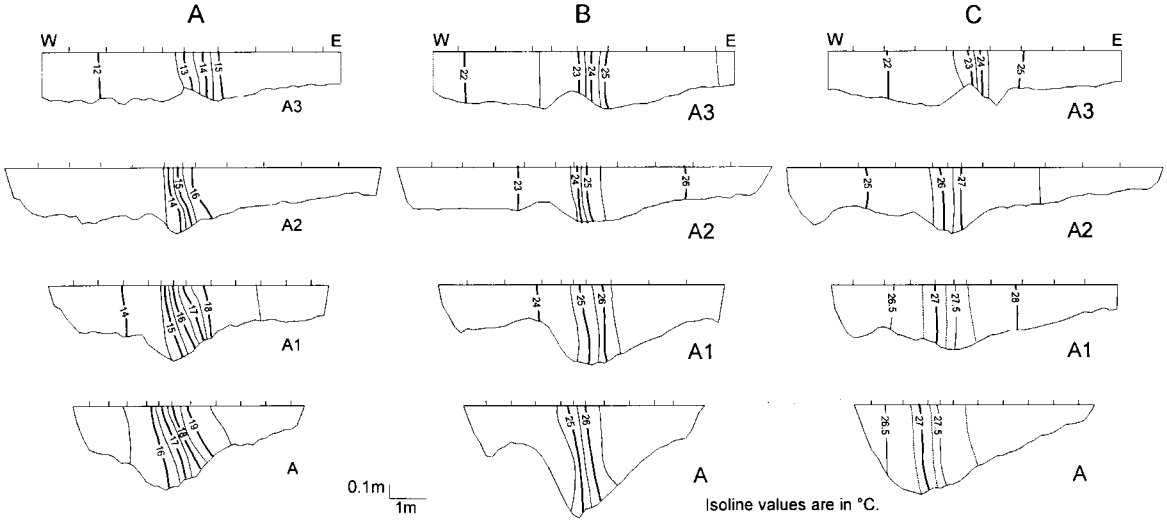

Figure 6. Water temperatures for (A) 7 June, (B) 8 July and (C) 27 July 1993. Ticks along water surface indicate locations of measurement verticals

advanced into the confluence, a prominent ridge developed along its leading edge immediately adjacent to the scour hole. Between 8 July and 27 July a series of high-stage events produced aggradation on the east side of the confluence and erosion of the sandy sediment lobe on the west side of the confluence. As a result, the scour hole shifted towards the west bank and decreased in depth by about 0·2 m (Figures 4 and 5).

Water temperatures and mixing interface

The temperature of the Copper Slough was higher than that of the Kaskaskia River on all three dates. This contrast in temperatures provides a means of distinguishing the waters of the confluent streams and of identifying the time-averaged location of the mixing interface, which consists of a zone of closely spaced

© 1998 John Wiley & Sons, Ltd.

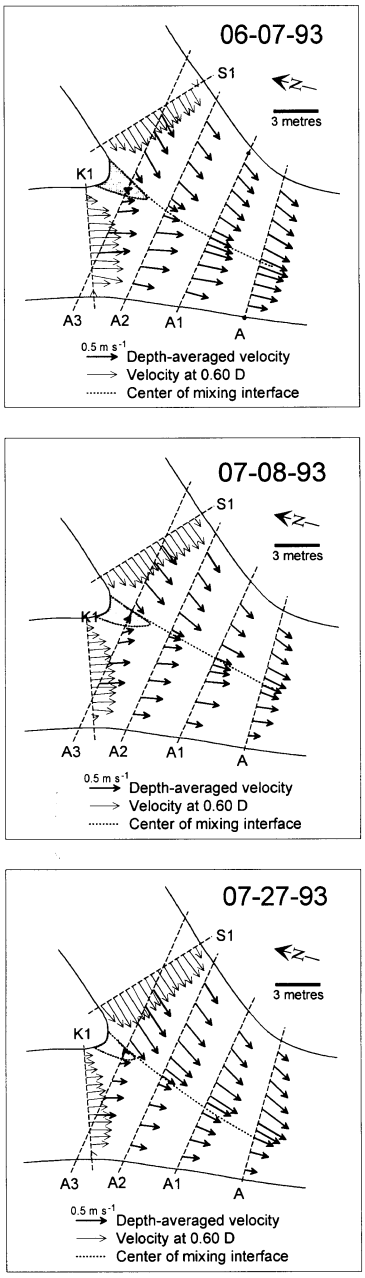

Figure 7. Depth-averaged velocity vectors, surficial position of the centre of the mixing interface, and region of recirculating flow near upstream junction corner (shaded) on 7 June, 8 July and 27 July 1993

isotherms within each cross-section (Figure 6). The temperature difference ($\Delta T = T_c - T_k$) was approximately 2·5°C at the beginning of each set of measurements, but by completion had increased to 3·5°C on 7 June and decreased to 1·0°C on 27 July. Trends in ΔT on 7 June and 27 July are apparent from spatial patterns of temperature at cross-sections A3 to A, which correspond to measurements obtained at successively later times of the day. The number of isotherms within the mixing interface increases at successive cross-sections on 7 June, whereas it decreases downstream on 27 July. On 8 July the temperature difference remained fairly constant throughout the day and the number of isotherms delimiting the mixing interface is uniform among the cross-sections.

 © 1998 John Wiley & Sons, Ltd.

On all three dates the mixing interface is vertical and located near the junction apex at the upstream end of the confluence (Figure 6). Further downstream, the position of the interface coincides with the location of the scour hole. On 7 June, the vertical orientation of the mixing interface clearly changes in the downstream direction as the portion of the isotherms near the surface becomes displaced towards the west bank relative to the portion near the bed. On the other two dates, the mixing interface remains nearly vertical in the downstream direction, although slight near-bed divergence of the isotherms is evident at cross-section A on 8 July and a slight inward displacement of the near-bed portion of the isotherms occurs at this same cross-section on 27 July.

Depth-averaged flow fields and path of the mixing interface

On all three dates, flow enters the confluence essentially parallel to the direction of the upstream channels. Velocity vectors at $0{\cdot}6D$ along cross-sections K1 and S1 for the most part are parallel to one another and have small cross-stream components (Figure 7). Velocities close to the banks near the junction apex are small, but positive, and reflect the combined influences of bank friction and the proximity of the near-bank flow to the stagnation zone immediately downstream.

On each date, a stagnation zone bounded by distinct shear layers and characterized by recirculating fluid developed at the junction apex, producing a velocity vector with a small ($\leq 0{\cdot}05\,\mathrm{m\,s^{-1}}$) magnitude and upstream or cross-stream orientation at the fifth vertical from the west bank at cross-section A3 (Figure 7). Depth-averaged velocities adjacent to the stagnation zone are small, reflecting convergence of slow near-bank fluid from the upstream channels along the margins of this zone. Immediately downstream of the stagnation zone, at cross-section A2, low-speed fluid from each channel flanks the mixing interface. Depth-averaged velocities along the mixing interface increase as the combining flows move towards the downstream channel.

The overall pattern of the depth-averaged velocity vectors is strongly convergent. Convergence is most pronounced at the upstream end of the confluence and decreases downstream as the streams mutually deflect one another and curve to enter the downstream channel. Deflection of flow at the upstream end of the confluence is greatest adjacent to the mixing interface. As flow moves towards the downstream channel, the pattern of deflection propagates outwards towards each bank.

Differences in the position of the mixing interface and overall orientations of the velocity vectors on each date reflect differences in the relative amount of deflection of each stream. The degree of deflection is related both to momentum ratio and to morphologic conditions. When $M_r > 1{\cdot}0$ (27 July) deflection of the Kaskaskia River by the Copper Slough is most pronounced and maximum depth-averaged velocities on the east side of the mixing interface exceed those on the west side. In contrast, when $M_r < 1{\cdot}0$ (7 June) deflection of the Kaskaskia River is less pronounced and maximum depth-averaged velocities on the west side of the mixing interface are greater than those on the east side. Consideration of M_r alone suggests that deflection of the Kaskaskia River on 8 July should be greater than that on 7 June, since M_r is higher on 8 July than on 7 June. In fact, deflection of the Copper Slough is greater and flow from the Kaskaskia River occupies a larger portion of the confluence width on 8 July than on 7 June. In addition, the path of the mixing interface is nearly linear on 8 July, whereas it curves noticeably on 7 June. This apparent anomaly can be explained by the influence of bed morphology on flow conditions. Between 7 June and 8 July the scour hole deepened and shifted eastwards as the lobe of sediment from the Kaskaskia River advanced into the confluence. Together these changes produced a decrease in channel capacity on the west side of the confluence and an increase in capacity on the east side, a pattern of bed topography that on 8 July forced incoming flow on the west (Kaskaskia) side of the confluence towards the scour hole. This topographic-forcing effect opposed deflection of the Kaskaskia flow to the west by the flow from the Copper Slough. Moreover, the increase in depth on the east side of the confluence allowed flow from the Copper Slough to be contained within a narrower portion of the confluence on 8 July than on 7 June, even though the Copper Slough discharge was similar on these two dates.

Downstream velocity fields

The general pattern of downstream velocity for each measured flow consists of a high-velocity core on each side of the mixing interface, one associated with each confluent stream. These cores are separated by a narrow zone of relatively low-velocity fluid near the centre of each cross-section (Figure 8). This low-velocity zone corresponds closely with the location of the mixing interface, and represents the coalesence of the regions of

© 1998 John Wiley & Sons, Ltd.

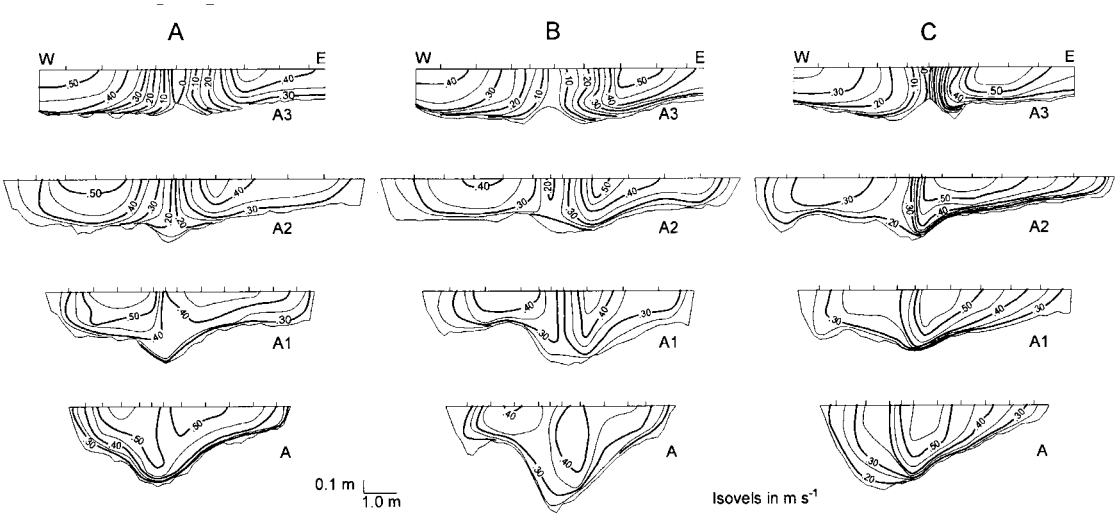

Figure 8. Downstream velocities for (A) 7 June, (B) 8 July and (C) 27 July 1993. Ticks along water surface indicate locations of measurement verticals

near-bank, low-velocity fluid from the upstream channels. Flow stagnation occurred near the centre of cross-section A3, especially on 7 June and 27 July when flow in this region was characterized by negative velocities (upstream flow). Velocities in the centre of the confluence increase downstream as the two high-velocity cores converge along the mixing interface. The high-velocity core associated with the dominant stream tends to expand into the region above the scour hole to a greater extent than the core associated with the subordinate stream.

The effect of momentum ratio on patterns of downstream velocity is illustrated by differences between the velocity fields on 7 June and 27 July. For 7 June, $M_r<1{\cdot}0$ and the high-velocity core on the west side of the mixing interface is larger and has higher maximum velocities than the relatively small high-velocity core on the east side of the confluence (Figure 8). Under these low momentum ratio conditions the low-velocity zone between the two high-velocity cores persists downstream to cross-section A; however, as the high-velocity cores converge in the downstream direction, the lateral gradient in downstream velocity in the centre of the confluence diminishes. Patterns of downstream isovels (Figure 8) suggest that transport of downstream momentum into the low-velocity region over the scour hole has a downward component in that the high-velocity core on the west side of the mixing interface develops a 'tongue' that progressively extends downwards into the zone of scour towards the downstream end of the confluence (cross-sections A1 and A). A similar pattern of downward inflection of the downstream isovels occurs at cross-section A for transport-effective flows with $M_r<1{\cdot}0$ (Rhoads, 1996), and the results here illustrate how this pattern evolves spatially upstream of this cross-section.

For the 27 July data, $M_r>1{\cdot}0$, and the downstream velocity field at the upstream end of the confluence again consists of two high-velocity cores separated by a low-velocity zone; however, the high-velocity core on the Copper Slough side of the mixing interface is shifted towards the centre of the confluence relative to its position on 7 June. This displacement produces a strong lateral gradient in downstream velocity along the mixing interface, suggesting that fluid shear was quite pronounced on this date. Towards the downstream end of the confluence, both the Kaskaskia high-velocity core and the adjacent low-velocity region are eliminated as the isovels surrounding the outward shifting Copper Slough high-velocity core merge with those of the Kaskaskia core. The presence of a single high-velocity core at cross-section A for $M_r>1{\cdot}0$ is consistent with previous observations of flow structure in the downstream portion of the CHZ at this confluence (Rhoads and Kenworthy, 1995). The spatial evolution of the downstream velocity field on the Copper Slough side of the

 © 1998 John Wiley & Sons, Ltd.

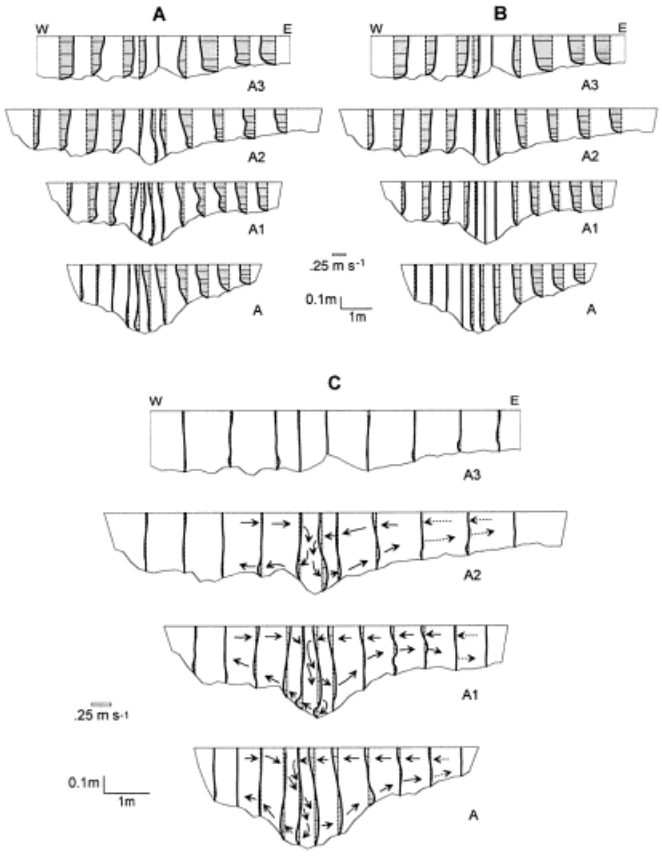

Figure 9. (A) Cross-stream velocities (v_y), (B) cross-stream component of primary velocities (v_{py}), and (C) cross-stream component of secondary velocities (v_{sy}) and patterns of secondary circulation (marked by arrows – see text for details), 7 June 1993. Horizontal lines at each vertical indicate the magnitude of the velocity component at measurement positions in the flow column

mixing interface on 27 July is similar to the sequence on the Kaskaskia side of the mixing interface on 7 June, suggesting that the degree to which one of the velocity cores penetrates downwards into the scour hole relative to the other depends on M_r.

For 8 July, $M_r \approx 1{\cdot}0$ and the pattern of downstream velocity is in some respects a combination of the patterns of 7 June and 27 July. As on 27 July, maximum velocities are highest on the Copper Slough side of the mixing interface and the Copper Slough core extends downwards into the scour hole as it shifts progressively towards this interface. The Copper Slough core does not combine with the Kaskaskia core towards the downstream end of the confluence; instead, two distinct high-velocity cores are evident at all four cross-sections. Also, isovels extend downwards into the scour hole on both sides of the mixing interface, suggesting that on this date both streams contributed to the downward transfer of downstream momentum into this region of the flow field.

Cross-stream velocity fields

The most prominent characteristic of the cross-stream velocity fields is the pronounced convergence of flow within the confluence (Figures 9–11). Cross-stream velocities on each side of the confluence generally are oriented towards the mixing interface. The high degree of similarity between the plots of v_{py}, which isolate the component of the cross-stream velocity field associated with skewing of the flow relative to the downstream direction at each cross-section, and the plots of v_y substantiates that the cross-stream velocity field is predominantly a product of flow convergence (Figures 9–11).

Variation in the direction of converging flow at each vertical is revealed by the cross-stream component of the secondary velocities (v_{sy}) (Figures 9–11). At some verticals, absolute values of v_{sy} are consistently less than

© 1998 John Wiley & Sons, Ltd.

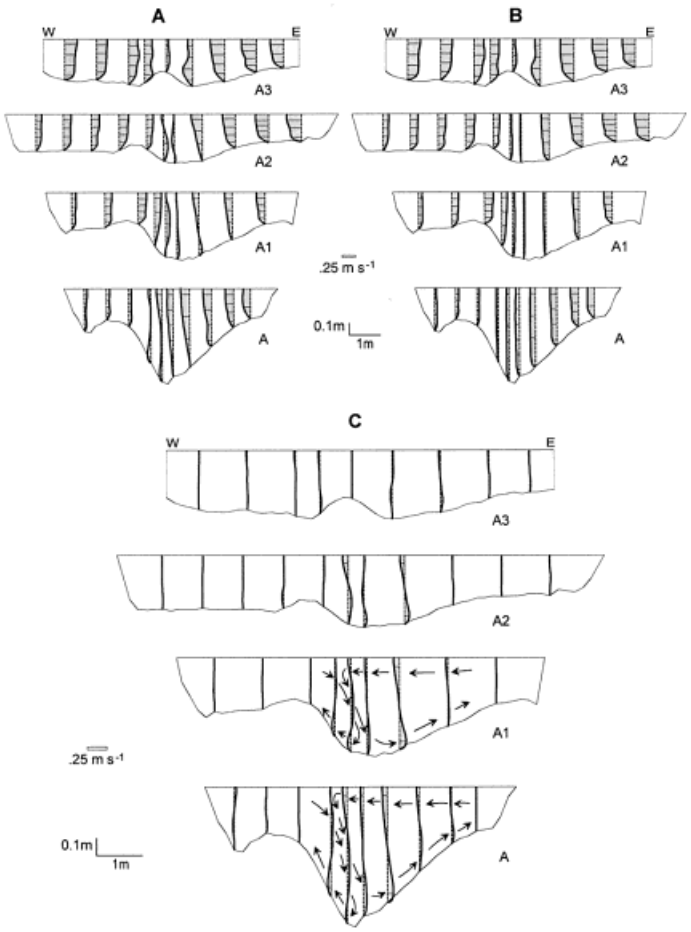

Figure 10. (A) Cross-stream velocities (v_y), (B) cross-stream component of primary velocities (v_{py}), and (C) cross-stream component of secondary velocities (v_{sy}) and patterns of secondary circulation (marked by arrows – see text for details), 8 July 1993. Horizontal lines at each vertical indicate the magnitude of the velocity component at measurement positions in the flow column

$0{\cdot}01\,m\,s^{-1}$, indicating that secondary circulation within the converging flow is virtually non-existent. Values this small are the same order of magnitude as instrument error. At other verticals, absolute values of v_{sy} are between $0{\cdot}015$ and $0{\cdot}10\,m\,s^{-1}$ and in many cases are the same order of magnitude as, or even exceed, absolute values of v_{py}. More important, values of v_{sy} at these verticals change systematically with depth, reflecting differences in the orientations of near-surface and near-bed velocity vectors of 10 to 20°, and also exhibit similar patterns of variation with depth at adjacent verticals, a characteristic that provides the basis for inferring the presence of coherent helical motion within the flow (Figures 9–11).

The solid arrows on Figures 9–11 were drawn based on the following criteria: (1) the maximum difference in values of v_{sy} at a vertical (Δv_{sy}) exceeds $0{\cdot}04\,m\,s^{-1}$ and the maximum difference in angles of orientation of velocity vectors (Δv) exceeds 5°; and (2) a systematic pattern of variation in v_{sy} is identifiable at two or more adjacent verticals. Vertical movement of fluid was inferred from abrupt changes in the direction of lateral flow at a particular depth and from the fact that the temperature data suggest that mixing of the two flows is largely confined to a distinct vertical band within the confluence (Figure 6). Dashed arrows were drawn where at least three adjacent verticals have a similar pattern of variation of v_{sy} with depth, Δv_{sy} exceeds $0{\cdot}025\,m\,s^{-1}$, and $\Delta\theta$ is greater than $3{\cdot}5°$.

Similarities in the spatial variation of v_{sy} for the three dates suggest that a consistent pattern of secondary circulation occurs within the confluence (Figures 9–11). This pattern consists of twin counter-rotating, surface-

 © 1998 John Wiley & Sons, Ltd.

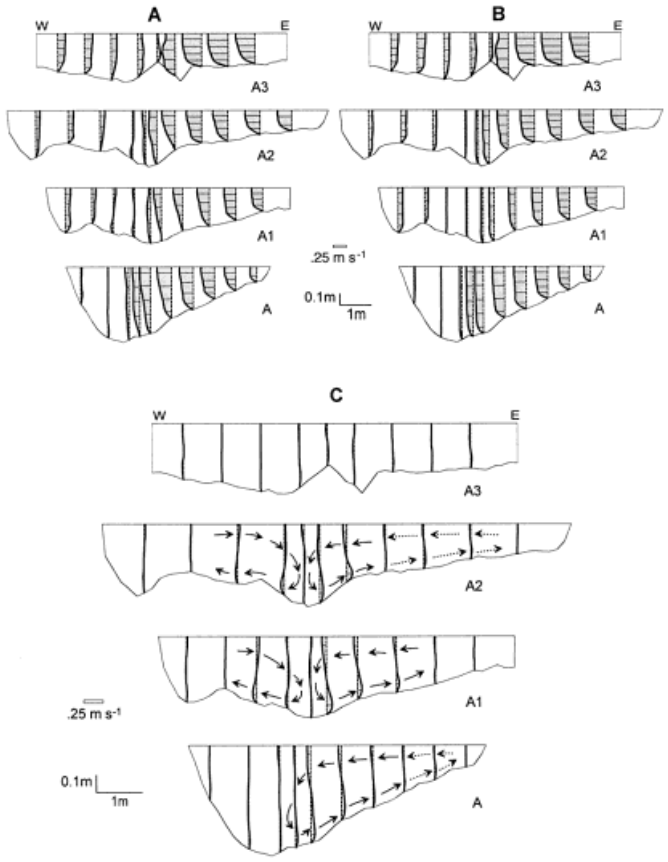

Figure 11. (A) Cross-stream velocities (v_y), (B) cross-stream component of primary velocities (v_{py}) and (C) cross-stream component of secondary velocities (v_{sy}) and patterns of secondary circulation (marked by arrows – see text for details), 27 July 1993. Horizontal lines at each vertical indicate the magnitude of the velocity component at measurement positions in the flow column

convergent helical cells on opposite sides of the mixing interface; clockwise (looking upstream) circulation occurs within the Kaskaskia portion of the flow, whereas counterclockwise motion is associated with the flow on the Copper Slough side of the mixing interface. Because the mixing interface marks the boundary between the two types of fluid motion, the spatial extent of each cell depends on M_r and bed morphology, which control the position of the mixing interface within the confluence. Thus, when the mixing interface is located near the centre of the confluence (7 June and 8 July), surface-convergent fluid motion along each side of this interface develops within the confluence (Figures 9 and 10). In contrast, when $M_r > 1{\cdot}0$ (27 July), weak clockwise circulation exists within the Kaskaskia flow at cross-sections A2 and A1, but this circulation dies out as the mixing interface shifts towards the west bank and counterclockwise circulation extends outwards towards the zone of maximum scour at cross-section A (Figure 11). These findings are consistent with previous work at this confluence which has shown that twin surface-convergent cells occur at cross-section A when $M_r \leq 1{\cdot}0$, and only a single cell exists when $M_r > 1{\cdot}0$ (Rhoads and Kenworthy, 1995; Rhoads, 1996). The counterclockwise cell on the Copper Slough side of the mixing interface also appears to override the weaker, less extensive cell on the Kaskaskia side of the mixing interface (Figure 9, cross-sections A1 and A; Figure 10, cross-sections A1 and A) – a phenomenon that has been observed in other studies of confluence flow structure (Ashmore *et al*., 1992).

The pattern of secondary circulation inferred from the v_{sy} is consistent with the downward transfer of downstream momentum over the scour hole inferred from the distortion of downstream isovels. Downward and inward expansion of the Kaskaskia high-velocity core over the scour hole is most pronounced when $M_r < 1{\cdot}0$ (7 June) and values of v_{sy} associated with clockwise circulation on the Kaskaskia side of the mixing interface are

© 1998 John Wiley & Sons, Ltd.

similar to or slightly greater than values of v_{sy} associated with counterclockwise motion on the Copper Slough side of the interface (Figures 8 and 9). Conversely, downward extension of the Copper Slough high-velocity core predominates when $M_r > 1{\cdot}0$ (27 July) and the strongest secondary circulation occurs on the Copper Slough side of the mixing interface (Figures 8 and 11). When $M_r \approx 1{\cdot}0$ (8 July), downward transfer of downstream momentum occurs on both sides of the interface (Figures 8 and 10). The consistency of these relations suggests that patterns of downstream velocity are strongly influenced by the development and relative strength of twin surface-convergent helical flow cells on opposite sides of the mixing interface.

DISCUSSION

The general pattern of two converging filaments of maximum downstream velocity separated by an intervening region of low-velocity fluid is consistent with conceptual models of flow in confluences (e.g. Bridge, 1993; Kenworthy, 1994), with measurements in anabranch confluences of a braided stream (Ashmore *et al*., 1992), and with patterns of flow observed in the downstream portion of this confluence when $M_r < 1{\cdot}0$ (Rhoads and Kenworthy, 1995; Rhoads, 1996). The results of this study illustrate in detail how this pattern evolves spatially within the confluence and how spatial evolution of this pattern varies with momentum ratio and with changes in bed morphology. Coalescence of the high-velocity cores occurs over a shorter spatial distance when $M_r > 1{\cdot}0$ than when $M_r < 1{\cdot}0$, which explains why previous work found that only a single core exists at the entrance to the downstream channel when $M_r > 1{\cdot}0$ (Rhoads and Kenworthy, 1995).

The presence of a narrow, well defined, approximately vertical thermal mixing interface at each cross-section indicates that little transverse mixing of the two incoming flows occurs within the confluence. This finding is consistent with results of experimental work, which has shown that the mixing interface is aligned vertically at confluences like this one where the bed elevations of the conjoining channels are concordant (Biron *et al*., 1996b). The vertical alignment of the mixing interface also explains the lack of appreciable transverse mixing of suspended sediment upstream of cross-section A at this confluence (Kenworthy and Rhoads, 1995). The mixing interface clearly corresponds to the low-velocity region separating the converging thalwegs of the two confluent streams; it is also a region of high fluid shear, at least at the upstream end of the confluence, as indicated by the strong lateral gradients of downstream velocity in this part of the flow field. The vertical orientation of the mixing interface in the central portion of the CHZ differs from its orientation in the downstream portion of the CHZ, where it becomes distorted towards the inner bank of the downstream channel (Rhoads and Kenworthy, 1995; Rhoads, 1996). Slight inclination of the mixing interface towards the inner bank is evident at the entrance to the downstream channel when $M_r < 1{\cdot}0$. Under these conditions, downward expansion of the Kaskaskia high-velocity core into the scour hole is predominant, suggesting that initial inclination of the mixing interface may in some cases be related to flow from the Kaskaskia River moving under flow from the Copper Slough.

The position of the mixing interface within the confluence depends in part on M_r. Increases in M_r shift the mixing interface away from the lateral tributary, whereas decreases in M_r move the interface towards this tributary – a relation that conforms with the results of experimental work (Best, 1987) and with theoretical considerations (Kenworthy and Rhoads, 1995). This general pattern, however, may be modified by the pattern of extant bed morphology, which, through continuity constraints, can topographically force incoming flow to move laterally within the confluence.

The field data also provide evidence for the existence of twin surface-convergent helical cells within the central region of this confluence – a phenomenon that has been documented for downstream portions of the CHZ in some (e.g. Mosley, 1976; Ashmore *et al*., 1992; Rhoads, 1996), but not all (e.g. Biron *et al*., 1993a, 1996b), previous studies. Theoretical considerations suggest that the pattern of weak secondary circulation identified in this study may be related to curvature of flow streamlines. The general pattern of circulation on all three dates, but especially on 7 June when $M_r < 1{\cdot}0$, is similar to that predicted by a computational fluid-dynamic model of flow through an asymmetrical confluence with a flat, concordant bed, a junction angle of 60°, and $M_r < 1{\cdot}0$ (Weerakoon *et al*., 1991). The development of twin surface-convergent cells in the numerical simulation is the result of mutual curvature of the two incoming flows within the confluence as they collide and deflect one another in opposite directions. The pattern of helical flow is similar to that in two meander bends placed back to

 © 1998 John Wiley & Sons, Ltd.

back (Rhoads, 1996); however, because the radial forces associated with streamline curvature are directed towards a region of mixing fluids, rather than a solid boundary, the transverse pressure gradient and intensity of secondary circulation are reduced compared to curving flows bounded by a solid bank (e.g. Weerakoon and Tamai, 1989).

The relation between orientations of the depth-averaged velocity vectors and patterns of v_{sy} also supports the hypothesis that systematic variation in v_{sy} is associated with curvature-induced helical motion. Patterns of v_{sy} consistent with helical motion are evident only at and/or downstream of cross-section A2 (Figures 9–11). The pattern of depth-averaged velocity vectors on all three dates shows that little or no curvature of the depth-averaged flow occurred between the upstream cross-sections and cross-section A3 (Figure 7). Noticeable reorientation of the depth-averaged vectors is evident between cross-sections A3 and A2, especially close to the mixing interface, where the magnitudes of v_{sy} for the two inferred counter-rotating cells are largest. Between cross-sections A2 and A, depth-averaged streamlines further away from the mixing interface begin to curve and secondary velocities in these portions of the flow increase (Figures 7 and 9–11).

Experimental work has suggested that apparent time-averaged helical motion can also be generated by separation of flow from the channel bed at discordant confluences (e.g. Best and Roy, 1991; Biron *et al*., 1996a,b). As flow enters a confluence from a discordant lateral tributary, it is drawn downwards over a region of separated flow in the lee of the tributary-mouth step, producing downwelling of flow in the centre of the confluence and upwelling at the downstream junction corner. Severe distortion of the mixing interface associated with this process may contribute to the overall pattern of fluid motion. Such a phenomenon could conceivably produce a time-averaged vectorial signature similar to that associated with a single helical cell, but which in fact is the time-averaged manifestation of intermittent shedding of large turbulent eddies from a distorted shear layer (Ferguson, 1993). Separation of flow from the bed might also occur at confluences with concordant beds if the central scour zone has steep enough side slopes to produce a large adverse pressure gradient (e.g. McLelland *et al*., 1996). In this case, downwelling and upwelling can occur on both sides of the mixing interface, the distortion of which depends on the relative strength of separation-induced secondary flow on each side of the confluence. In both the concordant and discordant cases, the key element is separation of flow from the bed due to abrupt changes in bed topography within the confluence.

The available evidence suggests that substantial separation of flow from the bed did not occur at the confluence for the flow conditions examined in this study. At each vertical, a velocity measurement was obtained at 5 cm below the water surface. The orientations of the velocity vectors at these near-surface positions will be affected least by minor bed irregularities, especially at measurement verticals upstream from the scour hole where the bed was relatively uniform. More important, near-surface vectors upstream from the scour hole are oriented more obliquely to the pattern of bed contours defining the region of scour than velocity vectors at any other position in the flow column. Thus, the orientations of the near-surface vectors provide an objective basis for assessing the potential for boundary-layer separation to occur as flow entering the confluence from each tributary encounters the side slopes of the scour hole.

The spatial rate of change in bed elevation along the path of the near-surface velocity vectors generally is less than 5° (Figure 12), an angle that is unlikely to induce substantial flow separation (Allen, 1982, p. 113). The maximum bed gradients along the path of the near-surface vectors occurred on 8 July where flow crossed the crest of the sediment lobe on the west side of the confluence. Local gradients at this location were between 7° and 9° (Figure 12), values much less than bed gradients over subaqueous gravitationally controlled avalanche faces (30 to 35°), such as those on the leeside of dunes, which induce substantial flow separation and the development of open or closed separation vortices. Recent work by Kostaschuk and Villard (1996), for example, showed that flow separation does not occur downstream of dunes with lee slopes of 12°. Values of v_{sy} in the lee of the sediment face on 8 July are not the largest that occur within the confluence on the three dates, or even the largest that occur on the west side of the mixing interface (Figures 9–11), which they should be if separation of flow from the bed is the primary cause of secondary circulation.

The lack of flow separation from the bed does not imply that spatial variation in channel geometry has no influence on the three-dimensionality of the flow. The emphasis placed on helical motion should not obscure the fact that flow is directed predominantly towards the centre of the confluence by the planform of the conjoining streams and by the geometry of the scour hole (e.g. Roy *et al*., 1988). Convergence is also enhanced by a

© 1998 John Wiley & Sons, Ltd.

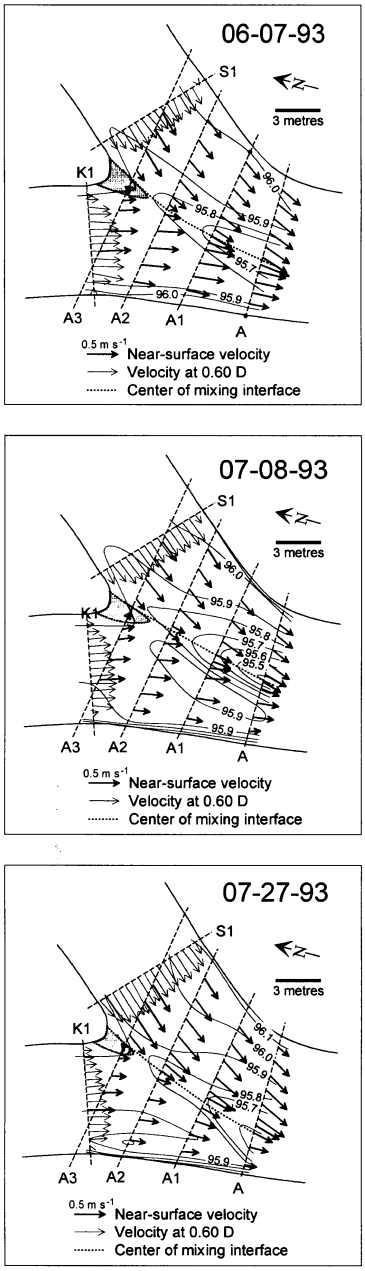

Figure 12. Near-surface velocity vectors on 7 June, 8 July and 27 July 1993

decrease in cross-sectional area of flow towards the downstream end of the confluence (Figures 9–11). As a result, the flow accelerates between cross-sections A2 and A by 10 per cent (8 July) to 30 per cent (7 June). This convective acceleration will stretch streamwise vorticity generated by skewing of the converging flows (i.e. curving of streamlines) as they mutually deflect one another (Perkins, 1970; Tennekes and Lumley, 1972, pp. 256–257). Accordingly, the intensity of secondary circulation in twin, surface-convergent helical cells will increase in the downstream direction, but especially in the cell on the lateral-tributary side of the confluence where the flow has a more consistent pattern and greater degree of curvature than flow on the main-stream side of the mixing interface (Figures 7 and 9–11) (Rhoads, 1996). This ‘spinning-up’ (Bradshaw, 1987) of the

 © 1998 John Wiley & Sons, Ltd.

tributary-side vortex will intensify as flow enters the downstream channel, resulting in distortion of the mixing interface towards the inner (east) bank of this channel (Rhoads and Kenworthy, 1995; Rhoads, 1996). The intensity of helical motion will eventually diminish as flow decelerates after passing the loci of maximum constriction associated with a lateral flow-separation zone and/or the presence of a tributary-side, lateral bar (e.g. Rhoads and Kenworthy, 1995; Neary and Odgaard, 1996).

Because the measurements reported in this paper were obtained for transport-ineffective conditions, their geomorphic significance is uncertain. Any assertions regarding the implications of the observed flow structure for sediment transport and the evolution of bed morphology at the confluence must be viewed as conjectural rather than definitive. Nevertheless, it is interesting to note that documented changes in bed morphology at the confluence are consistent with patterns of erosion and deposition likely to occur during transport-effective flows that are dynamically similar to the measured flows. In general, downward advection of high-velocity, near-surface fluid along the flanks of the mixing interface should generate high mean bed shear stresses and promote scour. Turbulence associated with a well developed shear layer probably also contributes to scour in this region (Biron *et al*., 1993a). Intensification of surface-convergent helical motion can lead to divergent flow near the bed, which facilitates scour-hole development by moving sediment away from the mixing interface (Rhoads, 1996). Thus, changes in the location of the mixing interface, which for formative events is directly related to the momentum ratio, should produce corresponding changes in the location of the scour hole. As momentum ratio increases, the mixing interface and zone of scour will move towards the outer (west) bank; as it decreases, the interface and zone of scour will move towards the mouth of the lateral tributary (e.g. Best, 1987). This hypothetical relation is supported by evidence on morphologic changes at the field site. During the several formative events that occurred prior to 7 June, the discharge of the Copper Slough exceeded that of the Kaskaskia River. The location of the scour hole on this date (slightly to the west of the channel centreline) is consistent with the expected location for $M_r > 1{\cdot}0$ (Figures 4 and 5). In contrast, M_r was less than one for extended periods following high flows in late June and early July (Figure 3). The eastward shift in the scour hole between 7 June and 8 July conforms with the eastward shift in the location of the mixing interface associated with a decrease in M_r (Figures 4, 5 and 7). During mid- to late July, storm events occurred mostly in the Copper Slough basin, resulting in a return to $M_r > 1{\cdot}0$ and, as expected, migration of the scour hole towards the west bank between 8 July and 27 July (Figures 4 and 5).

CONCLUSION

This study has produced detailed, quantitative information on the time-averaged flow structure within the central portion of an asymmetrical stream confluence under a variety of low-stage conditions. Major findings include the following.

(1) Patterns of water temperature reveal a narrow, well defined mixing interface within the confluence, suggesting that lateral mixing of the confluent flows is limited upstream of the entrance to the downstream channel.
(2) The position of the mixing interface reflects changes in the relative deflection of the streams as momentum ratio varies. The topographic influence of large-scale bed features on the geometry of transport-ineffective flow can also influence the path of the interface through the confluence.
(3) Depth-averaged velocity vectors and patterns of cross-stream velocity show that strong flow convergence occurs within the central region of the confluence. Flow convergence decreases in the downstream direction as the confluent flows mutually deflect one another and enter the downstream channel.
(4) Downstream velocity fields within the junction consist of two distinct high-velocity zones that converge along the mixing interface between the confluent streams. Near the junction apex, the high-velocity zones are separated by a region of low-velocity or recirculating fluid. The high-velocity core associated with the dominant stream tends to extend downwards into the scour hole in the downstream direction.
(5) Cross-stream components of secondary velocities suggest that twin surface-convergent helical flow cells exist within the flow with the two cells located on opposite sides of the mixing interface. This pattern is consistent with expected patterns of curvature-induced secondary circulation at asymmetrical confluences (Rhoads, 1996).

© 1998 John Wiley & Sons, Ltd.

(6) Changes in downstream velocity fields and in the pattern of helical motion reflect shifts in the position of the mixing interface as M_r varies. As M_r increases from less than one to greater than one, the spatial extent and strength of secondary circulation on the lateral-tributary side of the mixing interface increases, the extent and intensity of circulation on the main-stream side of the mixing interface decreases, and downward transfer of downstream momentum shifts from the main-stream side to the lateral-tributary side of the confluence.

Although this study suggests that streamline curvature can generate time-averaged helical flow at asymmetrical confluences, field measurements of three-dimensional instantaneous velocity components are needed to verify the existence of streamwise vortices, to link these vortices, if present, to generative mechanisms, and to uncover interactions among various coherent structures within and outside of the mixing interface. Ideally, such measurements should be obtained during channel-forming events to establish physical connections among flow patterns, sediment transport and dynamic changes in confluence morphology. Future research of this type will foster an improved understanding of geomorphic processes at stream confluences and of the role that confluences play in network-scale fluvial dynamics.

ACKNOWLEDGEMENTS

Dan Mayer and Phil Rathke assisted in the collection of the field data. Special thanks go to Jane Domier for her invaluable assistance with the figures. This research was supported by grants from the National Science Foundation (SES-9024225) and the University of Illinois Research Board. Comments by Colin Thorne and Jim Best on an earlier draft of this manuscript are greatly appreciated.

REFERENCES

Allen, J. R. L. 1982. *Sedimentary structures: Their Character and Physical Basis*, Volume II, Elsevier, Amsterdam. 663 pp.

Ashmore, P. E., Ferguson, R. I., Prestegaard, K. L., Ashworth, P. J. and Paola, C. 1992. 'Secondary flow in anabranch confluences of a braided, gravel-bed stream', *Earth Surface Processes and Landforms*, **17**, 299–311.

Bathurst, J. C., Thorne, C. R. and Hey, R. D. 1977. 'Direct measurements of secondary currents in river bends', *Nature*, **269**, 504–506.

Bathurst, J. C., Thorne, C. R. and Hey, R. D. 1979. 'Secondary flow and shear stress at river bends', *Journal of the Hydraulics Division, ASCE*, **105**, 1277–1295.

Best, J. L. 1987. 'Flow dynamics at river channel confluences: implications for sediment transport and bed morphology', in Ethridge, F. G., Flores, R. M. and Harvey, M. D. (Eds), *Recent Developments in Fluvial Sedimentology*, Society of Economic Paleontologists and Mineralogists, Special Publication, **39**, Tulsa, Oklahoma, 27–35.

Best, J. L. 1988. 'Sediment transport and bed morphology at river channel confluences', *Sedimentology*, **35**, 481–498.

Best. J. L. and Roy, A. G. 1991. 'Mixing layer distortion at the confluence of channels of different depth', *Nature*, **350**, 411–413.

Bevington, P. R. 1969. *Data Reduction and Error Analysis for the Physical Sciences*. McGraw-Hill, New York, 336 pp.

Biron, P., De Serres, B., Roy, A. G. and Best, J. L. 1993a. 'Shear layer turbulence at an unequal depth confluence', in Clifford, N. J., French, J. R. and Hardisty, J. (Eds), *Turbulence: Perspectives on Flow and Sediment Transport*, Wiley, New York, 197–213.

Biron, P., Roy, A. G., Best, J. L. and Boyer, C. J. 1993b. 'Bed morphology and sedimentology at the confluence of unequal depth channels', *Geomorphology*, **8**, 115–129.

Biron, P., Best, J. L. and Roy, A. G. 1996a. 'Effects of bed discordance on flow dynamics at open channel confluences', *Journal of Hydraulic Engineering*, **122**, 676–682.

Biron, P., Roy, A. G. and Best, J. L. 1996b. 'Turbulent flow structure at concordant and discordant open-channel confluences', *Experiments in Fluids*, **21**, 437– 446.

Bradshaw, P. 1987. 'Turbulent secondary flows', *Annual Review of Fluid Mechanics*, **19**, 53–74.

Bridge, J. S. 1993. 'The interaction between channel geometry, water flow, sediment transport and deposition in braided rivers', in Best, J. L. and Bristow, C. S. (Eds), *Braided Rivers*, Geological Society of London, Special Publication, **75**, 13–71.

Bristow, C. S., Best, J. L. and Roy, A. G. 1993. 'Morphology and facies models of channel confluences', in Marzo, M. and Puidefabregas, C. (Eds), *Alluvial Sedimentation*, Special Publication of the International Association of Sedimentologists, **17**, 91–100.

Ferguson, R. I. 1993. 'Understanding braiding processes in gravel-bed rivers: progress and unresolved problems', in Best, J. L. and Bristow, C. S. (Eds), *Braided Rivers*, Geological Society of London, Special Publication **75**, 73–87.

Gaudet, J. M. and Roy, A. G. 1995. 'Effect of bed morphology on flow mixing length at river confluences', *Nature*, **373**, 138–139.

Kenworthy, S. T. 1994. *Hydrologic and morphologic influences on confluence flow structure*, MSc thesis, Department of Geography, University of Illinois, 105 pp.

Kenworthy, S. T. and Rhoads, B. L. 1995. 'Hydrologic control of spatial patterns of suspended sediment concentration at a stream confluence', *Journal of Hydrology*, **168**, 251–263.

Kostaschuk, R. and Villard, P. 1996. 'Flow and sediment transport over large subaqeous dunes: Fraser River, Canada', *Sedimentology*, **43**, 849–863.

 © 1998 John Wiley & Sons, Ltd.

Mayer, D. R. 1995. *Hydrologic control of spatial patterns of surficial bed-material characteristics at a stream confluence,* MSc thesis, Department of Geography, University of Illinois, 120 pp.

McLelland, S. J., Ashworth, P. J. and Best, J. L. 1996. 'Origin and development of flow structures at junctions', in Ashworth, P. J., Bennett, S. J., Best, J. L. and McLelland, S. J. (Eds), *Coherent Flow Structures in Open Channels: Origins, Scales and Interactions with Sediment Transport and Bed Morphology,* Wiley, Chichester, 459–490.

Mosley, M. P. 1976. 'An experimental study of channel confluences', *Journal of Geology,* **84**, 535–562.

Neary, V. S. and Odgaard, A. J. 1996. 'Three-dimensional flow structure at open-channel diversions: closure', *Journal of Hydraulic Engineering,* **122**, 88–90.

Perkins, H. J. 1970. 'The formation of streamwise vorticity in turbulent flow', *Journal of Fluid Mechanics,* **44**, 721–740.

Rhoads, B. L. 1996. 'Mean structure of transport-effective flows at an asymmetrical confluence when the main stream is dominant', in Ashworth, P. J., Bennett, S. J., Best, J. L. and McLelland, S. J. (Eds), *Coherent Flow Structures in Open Channels: Origins, Scales and Interactions with Sediment Transport and Bed Morphology,* Wiley, Chichester, 491–517.

Rhoads, B. L. and Kenworthy, S. T. 1995. 'Flow structure at an asymmetrical stream confluence', *Geomorphology,* **11**, 273–293.

Roy, A. G. and Bergeron, N. 1990. 'Flow and particle paths at a natural river confluence with coarse bed material', *Geomorphology,* **3**, 99–112.

Roy, A. G., Roy, R. and Bergeron, N. 1988. 'Hydraulic geometry and changes in flow velocity at a river confluence with coarse bed material', *Earth Surface Processes and Landforms,* **13**, 583–598.

Tennekes, H. and Lumley, J. L. 1972. *A First Course in Turbulence,* MIT Press, Cambridge, MA, 300 pp.

Thorne, C. R. and Hey, R. D. 1979. 'Direct measurements of secondary currents at a river inflexion point', *Nature,* **280**, 226–228.

Weerakoon, S. B. and Tamai, N. 1989. 'Three-dimensional calculation of flow in river confluence using boundary-fitted coordinates', *Journal of Hydroscience and Hydraulic Engineering,* **7**, 51–62.

Weerakoon, S. B., Kawahara, Y. and Tamai, N. 1991. 'Three-dimensional flow structure in channel confluences of rectangular section', *Proceedings XXIV Congress, International Association for Hydraulic Research,* A, 373–380.

© 1998 John Wiley & Sons, Ltd.